# Plasma-Assisted Fabrication and Characterization of Magnetite Nanoparticles for Superparamagnetic Applications

## Soumen Mondal <sup>1</sup>, Dr. Devendra Pradhan <sup>2</sup>

Department of Physics, Mansarovar Global University, Sehore, M.P., India.

#### **ABSTRACT**

The diverse uses of magnetic nanoparticles in biomedicine, environmental cleanup, energy storage, and data recording systems have highlighted their relevance in the fast evolution of nanotechnology. Because of their biocompatibility, adjustable surface chemistry, and distinctive superparamagnetic characteristics, magnetite (Fe<sub>3</sub>O<sub>4</sub>) nanoparticles have garnered a lot of interest. The benefits of plasma-based synthesis over traditional chemical and physical approaches are shown in this work, which investigates magnetite nanoparticles that have been fabricated and characterized with the use of plasma. Instead of using harmful reducing agents, plasma-assisted procedures allow for more precise control over particle size, shape, crystallinity, and purity; this makes them a more environmentally benign option. To comprehend the connection between synthesis parameters and the magnetic characteristics that emerge, structural, morphological, and magnetic characterizations take center stage. The results show that Fe<sub>3</sub>O<sub>4</sub> nanoparticles made by plasma have a consistent shape, a small size distribution, and a strong magnetic response. These properties make them good candidates for uses like hyperthermia treatment, high-density data storage, controlled drug delivery, and MRI contrast agents. In order to facilitate their incorporation into next-generation superparamagnetic applications, this study shows that plasma-assisted synthesis provides a viable route for the sustainable, scalable, and repeatable production of magnetite nanoparticles.

**Keywords:** Plasma-Assisted Synthesis, Magnetite Nanoparticles, Superparamagnetism, Biomedical Applications, Sustainable Fabrication.

#### I. INTRODUCTION

With the ability to manipulate matter at the atomic and molecular size, nanotechnology has become one of the most impactful scientific disciplines. This has led to the development of new materials with distinct physical, chemical, and biological characteristics. Magnetite (Fe<sub>3</sub>O<sub>4</sub>) and other magnetic nanoparticles have garnered a lot of interest among nanomaterials because of their remarkable super paramagnetic behavior, how easy they are to functionalize, and the wide variety of uses they have in fields as diverse as data storage, wastewater treatment, and biomedical imaging. Magnetite nanoparticles are highly desirable for sensitive and reversible applications like biosensing and magnetic hyperthermia due to their superparamagnetism, a property where they show strong magnetization when exposed to an external magnetic field but lose remanence when the field is removed. Conventional methods for creating magnetite nanoparticles have relied on chemical processes such microemulsion, hydrothermal, sol-gel, and co-precipitation. Although these procedures are successful, they often have drawbacks such agglomeration, poor repeatability, and environmental impact from using harmful chemicals or surfactants. Physical procedures, such as ball milling or laser ablations, can provide options; however, they are sometimes very energy-intensive and do not allow for precise control of nanoscale characteristics.

A potent synthesis method that integrates energy efficiency, tunability, and environmental friendliness, plasma-assisted fabrication has arisen to conquer these obstacles. Ionized gases containing electrons, ions, and radicals may drive chemical processes at very low temperatures; this state of matter is generally

referred to as plasma. Controlled nucleation and development of nanoparticles are achieved by interactions between precursor materials and energetic plasma species in plasma-assisted manufacturing. Nanoparticles' size, shape, crystallinity, and surface functionality may be precisely controlled by adjusting reaction parameters such plasma power, gas composition, and exposure duration. Synthesis using plasma-assisted techniques is cleaner and more environmentally friendly since harmful reducing agents and stabilizers are not needed. New research has shown that compared to Fe<sub>3</sub>O<sub>4</sub> nanoparticles made using more traditional methods, those made using plasma had better magnetic characteristics, surface reactivity, and dispersion stability. Confirming the phase purity, crystallographic structure, shape, and magnetic performance of magnetite nanoparticles generated by plasma requires extensive characterization.

Multiple techniques are used, including X-ray diffraction (XRD), scanning electron microscopy (SEM), Fourier-transform infrared spectroscopy (FTIR), and vibrating sample magnetometry (VSM). The crystalline Fe<sub>3</sub>O<sub>4</sub> phase may be confirmed using XRD, and the nanoscale shape and particle size distribution can be seen using TEM and SEM. Biomedical conjugation and applications rely on FTIR studies for surface chemistry and functional group insights. Quantitative analysis of magnetic properties using VSM or SQUID magnetometry determines saturation magnetization, coercivity, blocking temperature, and degree of superparamagnetism. Nanoparticles of magnetite have use in many different fields. Nanoparticles of iron oxide have many uses in biomedicine, such as contrast agents in MRI scans, drug delivery vehicles, cancer hyperthermia treatment mediators, and biosensors for illness detection. Their ability to be externally directed or triggered without generating permanent magnetization in biological tissues is due to their superparamagnetic nature. Because of their high surface-to-volume ratio and magnetic retrievability, magnetite nanoparticles are used as effective adsorbents in environmental engineering to remove organic contaminants, heavy metals, and colors from polluted water. They have many applications in the energy and electronics industries, including catalysis in renewable energy processes, ferrofluids, and magnetic data storage systems.

Problems such as large-scale repeatability, long-term stability, and accurate surface modification to improve biocompatibility remain notwithstanding these potential uses. Many of these problems may be solved by plasma-assisted synthesis, which provides controlled growth conditions and yields nanoparticles with consistent properties. The industrial importance of plasma processes is further assured by their scalability via the use of atmospheric plasma reactors, plasma jets, or dielectric barrier discharges. This research primarily aims to characterize the structural and magnetic properties of Fe<sub>3</sub>O<sub>4</sub> nanoparticles that have been synthesized using plasma-assisted procedures. The study's goal is to show that this methodology has benefits over current approaches and that it can enable superparamagnetic applications by studying the influence of plasma settings on nanoparticle properties. The results will likely have farreaching implications for the development of eco-friendly nanofabrication methods and the broadening of magnetite nanoparticles' uses in fields as diverse as medicine, ecology, and industry.

#### **Superparamagnetic Applications of Magnetite Nanoparticles**

Magnetite nanoparticles (Fe<sub>3</sub>O<sub>4</sub>) have gained remarkable attention in recent years owing to their unique superparamagnetic properties, which make them highly suitable for a wide range of applications. Unlike bulk magnetic materials, superparamagnetic magnetite nanoparticles exhibit magnetization only in the presence of an external magnetic field and lose magnetization once the field is removed. This property eliminates the problem of particle agglomeration due to residual magnetism and makes them safe and efficient for biomedical and technological uses.

Superparamagnetic magnetite nanoparticles are predominantly utilized in biomedicine, namely for targeted medication delivery, magnetic resonance imaging (MRI), and hyperthermia treatment for cancer. In drug delivery systems, nanoparticles can be modified with therapeutic compounds and directed to certain tissues or tumors by an external magnetic field, thus reducing adverse effects on healthy tissues. Their robust contrast enhancement capability has rendered them extensively utilized as MRI contrast agents, providing superior image quality for diagnosis. In magnetic hyperthermia, magnetite nanoparticles produce localized warmth when subjected to an alternating magnetic field, efficiently annihilating cancer cells while preserving adjacent tissues.

Besides biomedical uses, magnetite nanoparticles exhibit considerable potential in environmental and industrial sectors. Their vast surface area and reactivity enable the adsorption of heavy metals, dyes, and other contaminants from wastewater, rendering them highly efficient in environmental remediation. Magnetite nanoparticles are utilized as reusable catalysts in catalysis for several chemical reactions, owing to their facile separation via an external magnet. In data storage and spintronics, their nanoscale dimensions and superparamagnetic properties facilitate the advancement of high-density magnetic storage systems with enhanced stability and performance.

Additionally, magnetite nanoparticles are being investigated for applications in biosensing and diagnostics. Functionalized nanoparticles can selectively attach to biomolecules, facilitating the detection of infections, DNA, or proteins with improved sensitivity. This use is essential for illness diagnostics, point-of-care testing, and the monitoring of biological processes.

The superparamagnetic characteristics of magnetite nanoparticles offer distinct benefits applicable to medical, environmental sustainability, industrial catalysis, and nanotechnology-based electronics. Their adjustable dimensions, capacity for surface modification, and biocompatibility guarantee that these nanoparticles will remain at the front of innovation in healthcare and technology.

#### II. LITERATURE REVIEW

Wiener, & Bassett, (2024) In this study, the interaction between navigation techniques is investigated in the context of route repetition, which involves repeating a route that has been travelled lately, and route retracing, which involves returning to the starting point of a route that has been travelled recently. It was during the learning phase that participants were moved along a route in a passive manner. They were then requested to repeat or retrace the journey so that they could participate in the test phase. During the learning phase, decision points were presented either in an order that was consistent with the learning phase (from the beginning to the end of the route repetition or from the end to the beginning of the route retracing), or in an order that was randomised. Participants' performance was superior when they were asked to repeat the path rather than retrace it, as was anticipated. It was shown that performance decreased when intersections were presented in a randomised order, which indicated that sequence knowledge had a role in route repetition and route retracing. The presentation of intersections in a sequence that is consistent with learning resulted in an improvement in performance, particularly on the initial portion of the route when the route was repeated. During the process of route retracing, this effect appeared to be absent. During route repetition and retracing, sequence information is utilized in a distinct manner, as demonstrated by these empirical findings. During the process of route repetition, we contend that participants resort to a tactic known as "sequence of turns" in addition to associating landmarks with changes in direction. Furthermore, we claim that it is highly improbable that route retracing is dependent on the same kind of sequence knowledge. Instead, we argue that route retracing makes use of information regarding the order in which choice points are reached. Taking everything into consideration, the findings

offer light on how navigators make use of sequence information for efficient navigation by highlighting a complex interplay of diverse tactics in route repetition and retracing.

Modi, Nimesh (2023) For the purpose of improving patient compliance and making administration more straightforward, Corona Remedies created the B-29 AQ PFS SC route. Both the pharmacokinetic behavior of methyl cobalamin subcutaneous injection and its non-inferiority to intramuscular injection will be explained by the findings of the study. This study aimed to compare two different injection formulations of methyl cobalamin, each with 1500 mcg, and assess their bioavailability, safety, and tolerability when given intramuscularly or subcutaneously. This was a randomized, two-treatment, parallel, comparative bioavailability research that was carried out on twenty-four adult human subjects who were healthy and normal by nature. Subcutaneous injections of 1500 mcg into the abdomen muscle or intramuscular injections into the gluteal muscle (buttock area) were used to provide the dosage of the investigational product (IP) after a minimum of a ten-hour fast the night before. Multiple blood samples were collected before and after the injection to ascertain the plasma methyl cobalamin levels. Area under the concentration-time curve (AUC), time to maximum plasma concentration (Tmax), and maximum plasma concentration (C) were all compared. Pharmacokinetic (PK) parameters were analyzed statistically using SAS (Statistical Analysis Software, Version 9.4 or later). Methylcobalamin had an average absorption time of 1.38 hours following subcutaneous (SC) administration and 1.49 hours following intramuscular (IM) administration. When comparing the bioavailability of subcutaneous and intramuscular injections, the ratio of the two procedures' population geometric averages is 103.62 for area under the curve. C was found to be bigger on the SC route (57.01 against 45.82) than on the IM route in this specific experiment.

Chou, Wei-Chun (2022) to estimate the dose of nanoparticles (NPs) on target organs and assess their hazards, physiologically based pharmacokinetic modeling—also known as PBPK modeling—is a crucial tool. In addition, there is a lack of both defined technique and systematic evaluation for building multiroute PBPK models for NPs. We postulated throughout this study that nanoparticles may not be wellmodeled using the standard route-to-route extrapolation approach to PBPK that is typically used for small molecule modeling. This study set out to answer that question by creating a multi-route PBPK model for adult rats that follows various routes of administration (i.e., intravenous (IV), oral gavage, intratracheal instillation, and endotracheal inhalation) for gold nanoparticles (AuNPs) ranging in size from 1.4 to 200 nm. Our model incorporates both the tried-and-true route-to-route extrapolation method for small molecules and a novel, route-specific data-based method that we suggest for NPs in general. Our research indicates that the PBPK model using this novel strategy outperformed its predecessor by a substantial margin. After the final PBPK model was fine-tuned using a Bayesian hierarchical approach and Markov chain Monte Carlo simulations, it was turned into a web-based interface using R Shiny. Multivariate linear regressions based on quantitative structure-activity relationships (QSAR) were established using the physicochemical parameters of AuNPs, including size, surface area, dosage, Zeta potential, and NP numbers. Important bio distribution parameters, such as the maximal uptake rate, that are route-specific were predicted using these regressions. It did not matter how the AuNPs were administered; what mattered most were their size and surface area, which determined the rates of endocytic and phagocytic absorption. In contrast, the estimation of exocytic release rates after intravenous injection was discovered to be significantly influenced by Zeta potential. Final thoughts It would appear that the traditional route-toroute extrapolation approaches that are commonly employed for PBPK modeling of small chemicals do not apply to NPs, according to the results of this study.

Abo Atia, Thomas (2016) To treat solutions that include heavy metals again, you need to do expensive procedures such using ionic exchange resins or activated carbon packed in fixed bed reactors. Use of magnetic nanoparticles as adsorbents may improve metal removal effectiveness, leading to the achievement of a relatively high specific surface area. Magnetic fields can also ease the final solid-liquid separation process, which eliminates the need for packed bed columns. The purpose of this research was to develop a straightforward synthetic method in order to manufacture copper nanoferrites (CuFe<sub>2</sub>O<sub>4</sub>) that are robust in water, magnetically active, and possess a high specific area. These nanoferrites are intended to be utilized as sorbent material for the removal of heavy metals from water solutions. Among the steps included in the hydrothermal process were surfactant-assisted coprecipitation (carried out at varying pH levels), hydrothermal treatment (carried out for one hour at 120 degrees Celsius), washing with water and hexane, drying, and sintering (carried out for one hour at 100 and 200 degrees Celsius). Studies were conducted to investigate the relationship between the coprecipitation pH (8, 10, and 12.5) and the sintering temperature (100-200 degrees Celsius) and the structure and sizes of CuFe<sub>2</sub>O<sub>4</sub> crystallites. The stability range in water was determined by conducting iron and copper release experiments at different pH levels. Potentiometric titrations were carried out to ascertain the net charge in respect to the bulk solution's pH. Without regard to the temperature at which the sintering was performed, the best samples in terms of magnetic properties were produced at a pH reading of 12.5. SEM images were used to estimate that the nanoparticles generated under these conditions had a mean size of between 35 and 45 nanometres.

Bhosale, Shivaji (2015) The experimental results relating to bovine serum albumin (BSA) adsorption on nickel ferrite (NiFe<sub>2</sub>O<sub>4</sub>) nanoparticles are detailed in this research. Ultimately, these investigations want to determine whether there is a relationship between the nanoparticles' microstructure, zeta potential, and adsorption capabilities. This study compares the physical properties of two varieties of nickel ferrites, one formed by chemical co-precipitation and the other by thermal plasma. The optimal pH-value for the greatest adsorption of BSA onto nickel ferrite nanoparticles was determined to be 5.58 at a body temperature of 37 degrees Celsius. The particles created by thermal plasma had a higher adsorption capacity (178.71 µg/mg) compared to the wet chemically generated ones. Over a wide pH range (3.64-0.96), the former was determined to have a higher zeta potential value than the latter, even when subjected to the same physical conditions. One possible explanation is that the two kinds of nanoparticles have different specific surface energies, which are affected by their degree of crystallinity. This research provides experimental proof that the thermal plasma-generated nanoparticles are single-crystalline, with an average size of 32 nm. This proof comes from particle-based electron diffraction and high-resolution transmission electron microscopy. Even though the X-ray diffraction patterns are not considerably different, the data show that the chemically generated particles have a poor crystalline shape with a mean size of 28 nm. Nuclear force microscopy pictures show that compared to chemically synthesized nanoparticles, those made utilizing plasma synthesis have a rougher surface. Vibrational spectroscopy confirmed the presence of adsorbed protein. Results from experiments show that the Langmuir adsorption model better fits the data than the Freundlich model.

Arora, Manisha & Sati, (2012) A gentle chemical process involving citric acid and tartaric acid routes, followed by low-temperature calcination, was used to produce the BiFeO3 nanoparticles. Based on structural characterization, it was determined that the two methods used to create pure phase were significantly different. In order to obtain pure phase BiFeO3 nanoparticles, the tartaric acid method was more effective than the citric acid technique, which required leaching in diluted nitric acid to eliminate impurity phases. Pure phase BiFeO3 nanoparticles synthesized by tartaric acid method underwent further optical, magnetic, and dielectric characterizations. A distorted rhombohedral structure was identified in

the BiFeO3 nanoparticles by the use of X-ray diffraction and Raman spectroscopy. Analysis of the BiFeO3 nanoparticles revealed that their average crystallite size varied between 30 and 50 nanometers. According to the findings of the UV-Visible diffuse absorption experiment, BFO nanoparticles had an impressive ability to soak up visible light ranging from 400 to 580 nm, with a threshold wavelength of 571 nm for absorption rates. Using absorption coefficient spectra as a calculation technique, the band gap of BiFeO3 nanoparticles was found to be 2.17 eV. Magnetic measurements revealed a saturated hysteresis loop, suggesting that room-temperature BiFeO3 nanoparticles are ferromagnetic. The temperature-dependent dielectric constant showed an outlier, which was determined to be much lower than the antiferromagnetic Néel temperature. This shows that BiFeO3 nanoparticles' antiferromagnetic Néel temperature has dropped significantly.

Yang, Hwami (2010) in this study, we reveal the size-controlled synthesis of BiFeO3 nanoparticles via a soft-chemistry technique. This approach successfully gels an aqueous solution of inorganic Bi and Fe salt by making use of acrylamide and bisacrylamide. It has been demonstrated that the grain size of the BiFeO3 powders may be tailored to individual needs by modifying the acrylamide to bisacrylamide proportion. Grain size decreases in a linear fashion as bisacrylamide concentration in the mixture increases. By using this process, many BiFeO3 samples with grain sizes ranging from 110 to 52 nm have been prepared. The thermal decomposition process of precursor xerogels and the generation of the BiFeO3 phase can be studied by X-ray diffraction; thermogravimetric analysis, differential scanning calorimetry analysis, and fourier transform infrared spectroscopy (FTIR). Using a scanning electron microscope (SEM), the produced BiFeO3 nanoparticles were seen to have a tiny and nearly spherical diameter distribution. The magnetic hysteresis loop measurement confirms that the BiFeO3 nanoparticles exhibit a little amount of ferromagnetic activity at room temperature. A saturation magnetization of approximately 1.56 emu/g is also achieved for the 52 nm sample.

#### III. EXPERIMENTAL SETUP

Iron oxide nanoparticle synthesis was carried out using the experimental setup shown in Fig.1. Operating the DC plasma at 250 amperes, the plasma gas was a 30/5 slm combination of helium and argon. Furrocene (Fe(CH)10) vapour served as the first component of the iron alloy. Although it remains a powder at ambient temperature, ferrocene takes on a sublime quality when heated. A heating mantle maintained a temperature of 120°C while the ferrocene was sublimated in a heated bed. Argon encased the ferrocene vapour as it passed across the heated bed at a speed of 0.5 slm. After adding oxygen to the heated bed, the mixture was fed into the plasma using a boron nitride converging nozzle that was located upstream. The fluid leaving the nozzle was forced into a chamber with a diameter of 250 mm and a pressure that was maintained between 40 and 53 kPa. To extend the high-temperature area for in-flight particle annealing, a ceramic tube of 356 mm in length, 32 mm in outer diameter, and 25 mm in inner diameter was positioned 51 mm above the nozzle exit. Injecting cold argon quench gas into the ceramic tube was the process. As independent variables, quench gas and oxygen flow rates were considered.

E-ISSN: 2582-9734

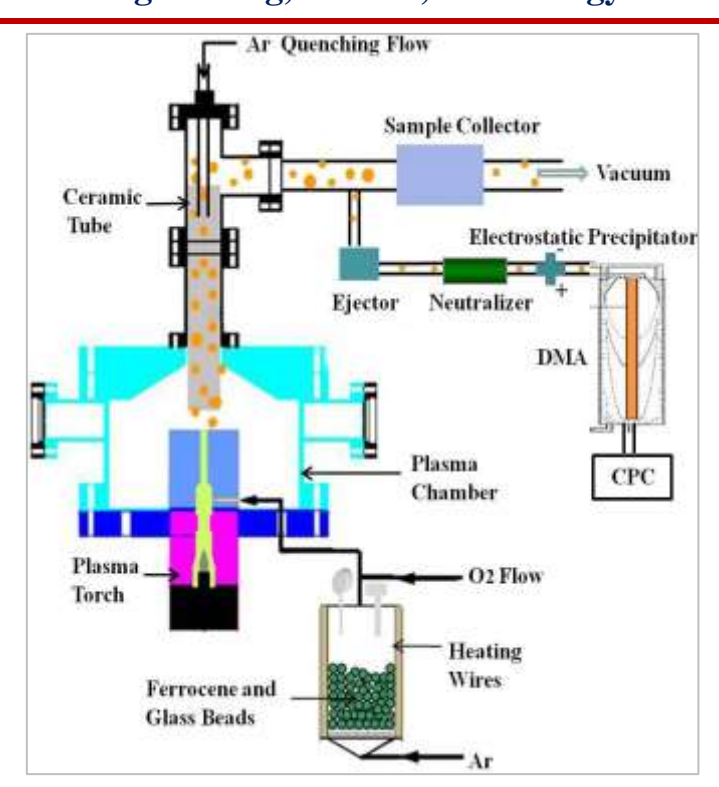


Figure 1: Experimental Apparatus Used for Synthesizing Super Paramagnetic Iron Oxide Nanoparticles

By recovering aerosol from the reactor exhaust using an ejector powered by high-pressure nitrogen, the size distribution of iron oxide nanoparticles generated in plasma was evaluated online using SMPS, which comprises a differential mobility analyzer and a condensation particle counter. The manufactured powder's chemical composition and magnetic characteristics were studied via off-line characterisation, which included collecting product nanoparticles on a glass fiber filter using a sample collector installed in the exhaust line. A Siemens D-500 diffraction meter powered by a 2.2 kW sealed cobalt source was used to conduct X-ray diffraction (XRD) experiments on the phase composition of the nanoparticles. At ambient temperature, a Princeton micro vibrating sample magnetometer was used to do magnetic measurements with a maximum applied field of one Tesla. Using a Tecnai G² F30 electron microscope, transmission electron microscopy (TEM) was used to study the nanoparticle shape. An electrostatic precipitator was used to collect TEM samples on lacey carbon grids. A bipolar charger, also known as a Po radiation source, was placed in the sampling line, and a voltage of 3 kV was delivered to the precipitator.

#### IV. RESULTS AND DISCUSSION

Using VSM, the magnetic characteristics of iron oxide nanoparticles produced in plasma were studied. At room temperature, hysteresis loops were tested with different oxygen flow rates (Fig. 2), while maintaining a constant ferrocene feeding rate of around 7.9 sccm. Sample mass as measured on the glass fiber filter was used to normalize magnetic moments. It is observed that the saturation magnetization is strongly affected by the oxygen flow rate. At 200 sccm, the saturation magnetization reached its peak at 28.4 emu/g. A characteristic of superparamagnetism is the absence of hysteresis in the curves, as measured to the nearest line thickness. At an oxygen flow rate of 200 sccm/s, the coercively was 22.1 Oe and the remanence was 1.87 emu/g. The saturation magnetization values for magnetite and maghemite are lower than the bulk values that have been reported. Phase impurities, especially the antiferromagnetic hematite phase, might be to blame for the reduced magnetism, as we'll see below.

E-ISSN: 2582-9734

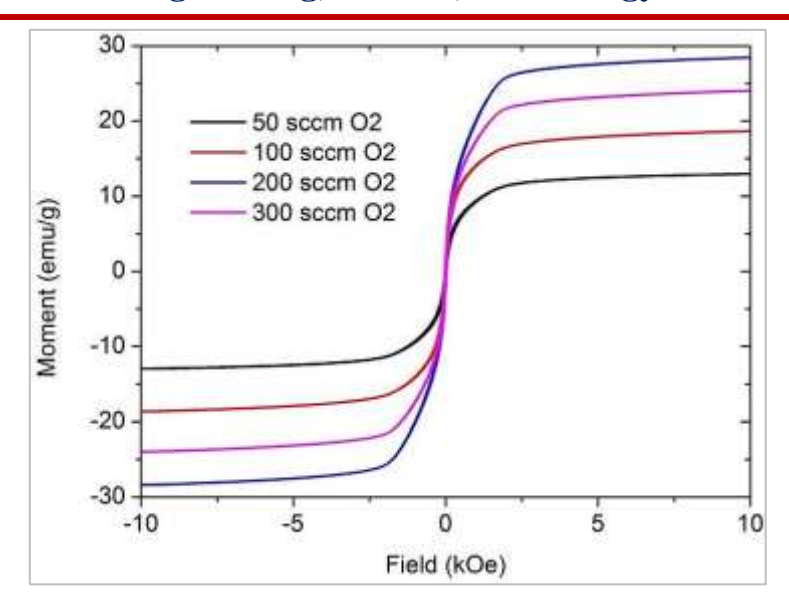


Figure 2: VSM Hysteresis Loops of Iron Oxide Nanoparticles Synthesized Under Different Oxygen Flow Rates

Figure 3 shows transmission electron microscopy (TEM) pictures of nanoparticles produced at 200 sccm of oxygen, without argon quenching flow. A big clump of iron oxide nanoparticles, with main particle diameters ranging from 5 to 8 nanometers, is seen in the transmission electron micrograph (TEM) picture in Figure 3(a), which is thought to have developed during deposition on the TEM grid. One iron oxide nanoparticle's lattice fringes are clearly visible in the high-resolution transmission electron micrograph (TEM) picture in Figure 3(b). The maghemite (310) plane corresponds to the d-spacing observed in the picture, which is about 2.65 Å.

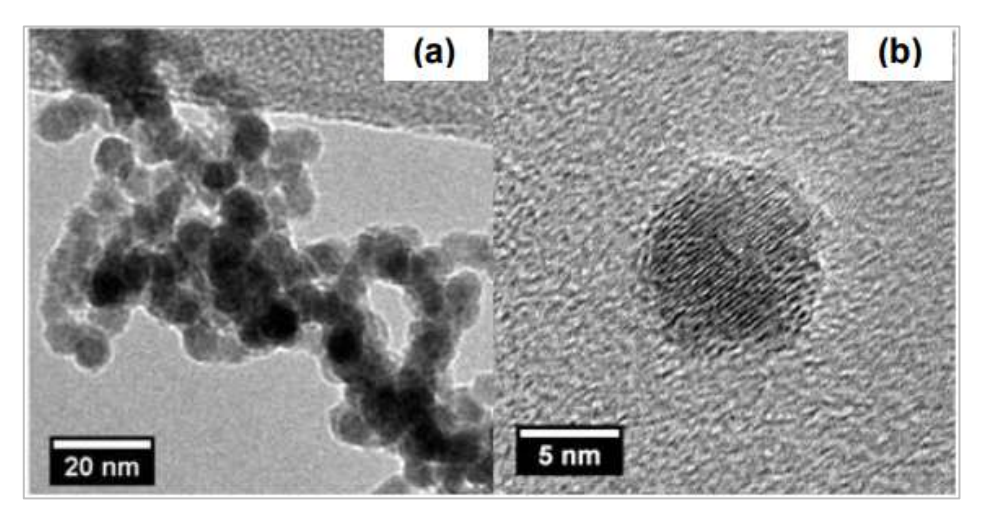


Figure 3: TEM Analysis of Plasma-Synthesized Iron Oxide Nanoparticles

Fig. 4 shows a comparison of the XRD pattern of magnetite and maghemite nanopowder bought from Sigma-Aldrich with that of plasma- generated iron oxide nanoparticles made at a 200 sccm oxygen flow rate with no argon quench flow. Due to hematite impurities, which may have been introduced by air, the normal maghemite Nano powder exhibits tiny peaks. The cubic structure and crystal lattice parameters of magnetite and maghemite are identical; the former has a value of 0.8396 nm while the latter has 0.83474 nm. You can't tell the two apart by looking at their XRD patterns. Figure 4 shows that magnetic nanoparticles made from plasma include both magnetite (and ma-ghemite) and hematite (an antiferromagnetic phase). If the product contains hematite, its average saturation magnetization will be lower. The high-temperature plasma process could be responsible for the hematite phase's development.

E-ISSN: 2582-9734

Hematite might also occur because the super paramagnetic iron oxide nanoparticles are unstable because of their tiny size. Upon exposure to air, the surfaces of these microscopic iron oxide nanoparticles may rapidly develop a thin coating of hematite.

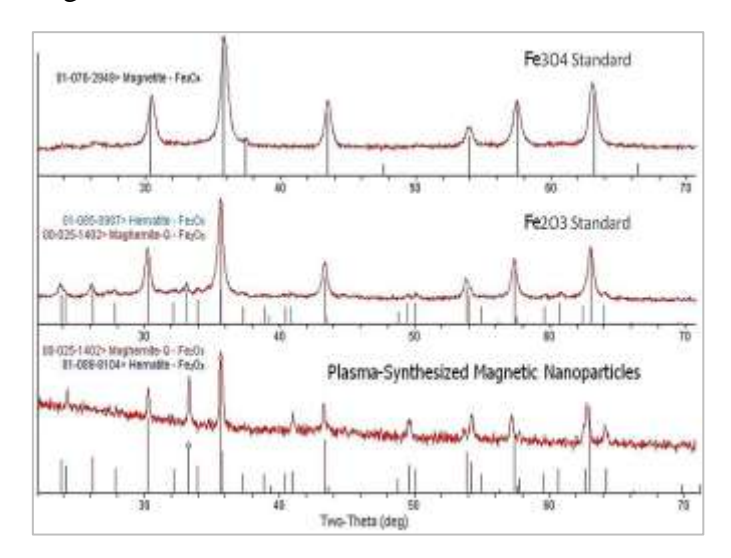


Figure 4: XRD Profiles of Plasma-Synthesized Iron Oxide Nanoparticles Alongside Magnetite and Sigma-Aldrich Standard

Figure 5 displays the measured size distributions of iron oxide particles generated in plasma as a function of different argon quench gas flow rates. Approximately 7.9 sccm of ferrocene vapor and 200 sccm of oxygen were used to create these particles. SMPS determines the particle mobility diameter, which might include agglomerates with many main particles. As the quench gas flow rate rises, the average particle size decreases, keeping the precursor feeding rate and oxygen flow rate constant. By increasing the quench gas flow rate from 0 to 30 slm, the mode of the size distributions in Fig. 5 shrinks from around 18 nm to around 12 nm.

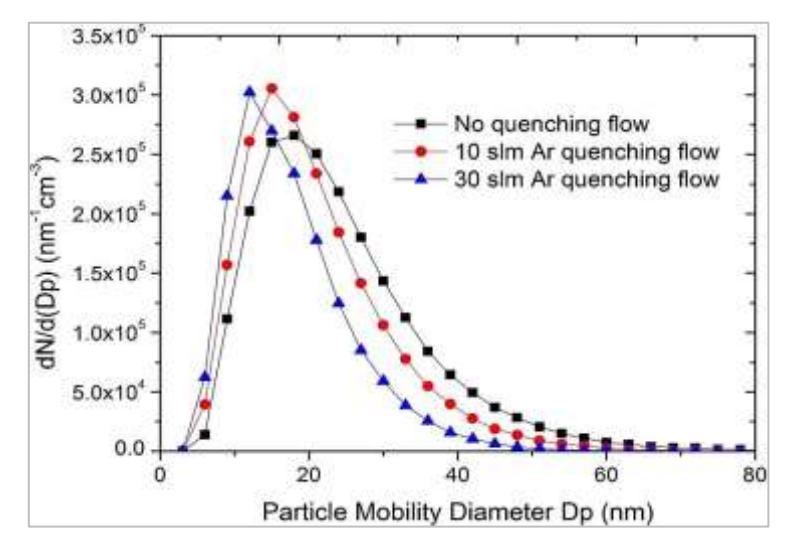


Figure 5: Particle Size Distribution Obtained by SMPS for Varying Argon Quench Gas Flow Rates

The synthesis of super paramagnetic iron oxide nanoparticles from ferrocene, an iron precursor, was accomplished utilizing a DC thermal plasma system. Nanoparticles of magnetic iron oxide produced by plasma typically have a size range of 5–8 nanometers. Although hematite is present, the powders mostly consist of the super paramagnetic magnetite (or magnetite) phase. This is the first research that we are aware of on the synthesis of super paramagnetic iron oxide nanoparticles using plasma, regardless of the kind of plasma used. By influencing the phase composition and iron oxide stoichiometry, the oxygen flow rate significantly alters the final powder's magnetic characteristics. One way to decrease the agglomeration size of magnetic iron oxide nanoparticles generated in plasma is to add argon to the reaction chamber. Each agglomeration comprises many parent particles, since the mean agglomerate size was around 16 nm at the greatest quench gas flow rate that was examined.

#### V. CONCLUSION

The inherent super paramagnetic characteristics and wide application possibilities of magnetite (Fe<sub>3</sub>O<sub>4</sub>) nanoparticles make them a very attractive class of nanomaterials. Despite their widespread usage, traditional physical and chemical synthesis methods have problems with agglomeration, environmental concerns, and repeatability. To overcome these issues, plasma-assisted manufacturing offers a sustainable and creative technique to regulate particle shape, crystallinity, and surface properties without using harmful chemicals. It has been confirmed by characterization methods that nanoparticles made of plasma have better structural integrity and magnetic behavior, which makes them applicable to biological, environmental, and technical fields. There is a growing need for green nanotechnology, and plasma-assisted technologies are a good fit since they are both environmentally benign and scalable. Exploring hybrid plasma-chemical processes, improving surface modifications for focused applications, and optimizing plasma parameters for large-scale synthesis are all potential future approaches. In conclusion, the characterisation and synthesis of magnetite nanoparticles using plasma-assisted methods provide the groundwork for the creation of next-generation super paramagnetic materials, which might lead to innovations in healthcare, sustainable development, and cutting-edge functional devices.

#### **REFERENCES**

- 1. J. Wiener, C. Bassett, S. Bentall, and C. Black, "EXPRESS: Interplay of wayfinding strategies in route repetition and route retracing," *Q. J. Exp. Psychol.*, vol. 78, no. 1, pp. 1–8, 2024.
- 2. N. Modi, A. Jaiswal, and P. N. S. S. Vasu, "Methylcobalamin injection 1500 mcg SC route versus IM route: A randomized parallel comparative bioavailability study," *IP Indian J. Neurosci.*, vol. 9, no. 3, pp. 141–147, 2023.
- 3. W.-C. Chou, Y.-H. Cheng, J. Riviere, N. Monteiro-Riviere, W. Kreyling, and Z. Lin, "Development of a multi-route physiologically based pharmacokinetic (PBPK) model for nanomaterials: A comparison between a traditional versus a new route-specific approach using gold nanoparticles in rats," *Part. Fibre Toxicol.*, vol. 19, no. 1, pp. 1–19, 2022.
- 4. A. Samrot, C. Sahithya, J. Selvarani, S. K. Purayil, and P. Paulraj, "A review on synthesis, characterization and potential biological applications of superparamagnetic iron oxide nanoparticles," *Curr. Res. Green Sustain. Chem.*, vol. 4, no. 5, pp. 10–42, 2020.
- 5. Y. Xiao and J. Du, "Superparamagnetic nanoparticles for biomedical applications," *J. Mater. Chem. B*, vol. 8, no. 2, pp. 1–10, 2019.
- 6. A. Ramzannezhad, P. Gill, and A. Bahari, "Fabrication of magnetic nanorods and their applications in medicine," *BioNanoMaterials*, vol. 18, 2017.

## International Journal of Engineering, Science, Technology and Innovation (IJESTI)

7. S. M. Abdollah, F. Fathi, and N. Farhadyar, "Synthesis and modification of iron oxide nanoparticles (magnetite) for biomedical applications," *Res. J. Biotechnol.*, vol. 12, no. 9, pp. 87–95, 2017.

E-ISSN: 2582-9734

- 8. T. A. Abo Atia, P. Altimari, E. Moscardini, I. Pettiti, L. Toro, and F. Pagnanelli, "Synthesis and characterization of copper ferrite magnetic nanoparticles by hydrothermal route," *Chem. Eng. Trans.*, vol. 4, no. 7, pp. 151–156, 2016.
- 9. J. Ibarra, J. Melendres, M. Almada, M. G. Burboa, P. Taboada, J. Juárez, and M. A. Valdez, "Synthesis and characterization of magnetite/PLGA/chitosan nanoparticles," *Mater. Res. Express*, vol. 2, no. 9, pp. 1–17, 2015.
- 10. S. Bhosale *et al.*, "Micro-structural analysis of NiFe<sub>2</sub>O<sub>4</sub> nanoparticles synthesized by thermal plasma route and its suitability for BSA adsorption," *J. Mater. Sci. Mater. Med.*, vol. 26, no. 8, pp. 1–15, 2015.
- 11. L. Feng, B. Zhang, and F. Zhao, "Preparation and characterization of superparamagnetic magnetite Fe<sub>3</sub>O<sub>4</sub> nanoparticles," *Polym. Mater. Sci. Eng.*, vol. 28, no. 8, pp. 144–147, 2012.
- 12. M. Arora, S. Sati, S. Chauhan, S. Chhoker, A. Panwar, and M. Kumar, "Structural, optical and multiferroic properties of BiFeO₃ nanoparticles synthesized by soft chemical route," *J. Supercond. Nov. Magn.*, vol. 26, no. 2, pp. 443–448, 2012.
- 13. H. Yang, Z. Wei, J. Dai, J. Jiang, and W. Feng, "Size-controlled synthesis of BiFeO<sub>3</sub> nanoparticles by a soft-chemistry route," *J. Sol-Gel Sci. Technol.*, vol. 58, no. 1, pp. 238–243, 2010.
- 14. M. Hofmann-Amtenbrink, B. von Rechenberg, H. Hofmann, and M. Tan, "Superparamagnetic nanoparticles for biomedical applications," *Adv. Drug Deliv. Rev.*, vol. 65, no. 2, pp. 1–9, 2009.
- 15. M. Babič *et al.*, "Poly(L-lysine)-modified iron oxide nanoparticles for stem cell labeling," *Bioconjug. Chem.*, vol. 19, no. 3, pp. 740–750, 2008.
- 16. A. Petri-Fink *et al.*, "Effect of cell media on polymer coated superparamagnetic iron oxide nanoparticles (SPIONs): Colloidal stability, cytotoxicity, and cellular uptake studies," *Eur. J. Pharm. Biopharm.*, vol. 68, pp. 129–137, 2008.
- 17. C. von Zur Mühlen *et al.*, "Superparamagnetic iron oxide binding and uptake as imaged by magnetic resonance is mediated by the integrin receptor Mac-1 (CD11b/CD18): Implications on imaging of atherosclerotic plaques," *Atherosclerosis*, vol. 193, no. 1, pp. 102–111, 2007.
- 18. B. R. Smith *et al.*, "Localization to atherosclerotic plaque and biodistribution of biochemically derivatized superparamagnetic iron oxide nanoparticles (SPIONs) contrast particles for magnetic resonance imaging," *Biomed. Microdevices*, vol. 9, no. 5, pp. 719–727, 2007.
- 19. D. L. Thorek *et al.*, "Superparamagnetic iron oxide nanoparticle probes for molecular imaging," *Ann. Biomed. Eng.*, vol. 34, no. 1, pp. 23–38, 2006.
- 20. M. Chastellain *et al.*, "Surface functionalization of superparamagnetic nanoparticles," *J. Colloid Interface Sci.*, vol. 278, pp. 353–360, 2004.
- 21. C. Alexiou *et al.*, "Targeting cancer cells: Magnetic nanoparticles as drug carriers," *Eur. Biophys. J.*, vol. 35, no. 5, pp. 446–450, 2006.
- 22. D. Horák, "Magnetic microparticulate carriers with immobilized selective ligands in DNA diagnostics," *Polymer*, vol. 46, no. 4, pp. 1245–1255, 2005.
- 23. A. K. Gupta and M. Gupta, "Synthesis and surface engineering of iron oxide nanoparticles for biomedical applications," *Biomaterials*, vol. 26, no. 18, pp. 3995–4021, 2005.
- 24. T. Neuberger *et al.*, "Superparamagnetic nanoparticles for biomedical applications: Possibilities and limitations of a new drug delivery system," *J. Magn. Magn. Mater.*, vol. 293, no. 1, pp. 483–496, 2005.

# Vol 5, Issue 4, April 2025 E-ISSN: 2582-9734 International Journal of Engineering, Science, Technology and Innovation (IJESTI)

- 25. A. Petri-Fink *et al.*, "Development of functionalized superparamagnetic iron oxide nanoparticles for interaction with human cancer cells," *Biomaterials*, vol. 26, no. 15, pp. 2685–2694, 2005.
- 26. K. Gupta and A. S. G. Curtis, "Lactoferrin and ceruloplasmin derivatized superparamagnetic iron oxide nanoparticles for targeting cell surface receptors," *Biomaterials*, vol. 25, no. 15, pp. 3029–3040, 2004.
- 27. Jordan *et al.*, "Presentation of a new magnetic field therapy system for the treatment of human solid tumors with magnetic fluid hyperthermia," *J. Magn. Magn. Mater.*, vol. 225, no. 1–2, pp. 118–126, 2001.